Supplementary Materials for:

From hot rock to useful energy: A global estimate of enhanced geothermal systems potential

Arman Aghahosseini* and Christian Breyer

LUT University, Yliopistonkatu 34, 53850 Lappeenranta, Finland

** Corresponding author - E-mail address: arman.aghahosseini@lut.fi*

1. EGS cost calculation method

The capital costs or capital expenditures (CAPEX) are calculated as the sum of the geothermal well drilling and completion costs ($C_{cap,well}$), the surface plant costs ($C_{cap,pp}$), the reservoir stimulation costs ($C_{cap,stim}$), the fluid distribution costs ($C_{cap,distr}$) and the resource exploration costs ($C_{cap,expl}$) [1], as summarised in Equation S1. In addition, a learning factor (*LF*) is applied to describe the specific technology learning, according to Equation S11a:

$$CAPEX(z, T_r, T_z, \eta_{th}, W, q_0, k, t, y_0, y_f) = \left(C_{cap,well}(z, T_z, q_0, k, t) \cdot n + \frac{C_{cap,pp}(T_r, T_z, \eta_{th}, W) \cdot W}{10^3} + C_{cap,stim} + C_{cap,distr}(T_z) + C_{cap,expl}(z, T_z, q_0, k) \right) \cdot LF(y_0, y_f) \quad \text{(S1)}$$

where z is the depth, T_r is the base temperature as presented in Equation 4 of the main article, T_z is the temperature at depth z, η_{th} is the net thermal efficiency, W is the power plant capacity for the year t in MW, q_0 is the surface heat flow, k is the thermal conductivity, t is the year, n is the number of wells (production and injections wells), and *LF* is the learning factor calculated based on the reference cost year (y_0) and the future cost year (y_f) according to Equation S11a.

Since the costs of geothermal wells are not widely discussed, a more concrete pattern for costs estimation of geothermal wells is needed. Lukawski et al. [2] proposed an equation that shows a rough estimation of the average current costs of geothermal wells, as shown in Equation S2.

$$C_{cap,well}(z, T_z, q_0, k, t) = 1.72 \times 10^{-7} \cdot z^2 + 2.3 \cdot 10^{-3} \cdot z - 0.62 \cdot \nabla T(T_z, q_0, k) \cdot C_{frac,drill}(t) \quad \text{(S2)}$$

where z is the measured depths of a well, which is assumed to be the same as the 1 km thick layer depth for simplicity, ∇T is the ratio of the geothermal gradient (ω) to the estimated geothermal gradient ($\omega_{estimated}$), as shown in Equation S3, and $C_{frac,drill}$ is the fraction of baseline drilling costs for the year t that is listed in Table S1. It is assumed that the fraction of baseline drilling costs decreases over time, as the drilling technology evolves [1]. The correlation coefficient R^2 is 0.92. This equation is adopted to gauge the geothermal well costs for each 1 km depth interval. The average costs of geothermal wells are obtained in USD.

$$\nabla T(z, T_z, q_0, k) = \frac{\omega(q_0, k)}{\omega_{estimated}(z, T_z)} \quad \text{(S3a)}$$

$$\omega(q_0, k) = \frac{q_0}{k} \quad \text{(S3b)}$$

$$\omega_{estimated}(z, T_z) = \frac{T_z}{z} \quad \text{(S3c)}$$

The surface power plant costs for 1- and 2-flash systems are calculated based on Equation S4:

$$C_{cap,pp}(T_r, T_z, \eta_{th}, t, W) = 750 + 1125 \cdot [\exp(-0.006115(W(T_z, T_r, \eta_{th}, t) - 5))] \quad \text{(S4)}$$

where W is the power plant capacity for the year t in MW, calculated from the exergy of geothermal fluid coming from the EGS reservoir at any temperature. The electricity production is obtained using Equation S5 [3]:

$$E(T_z, T_r, \eta_{th}, t) = Q(t) \cdot \rho_{water} \cdot Cp_{water} \cdot (T_z - T_r) \cdot \eta_{th}(T) \cdot 10^{-3} \cdot t_{load} \cdot CF \quad \text{(S5a)}$$

$$t_{load} = 8760 \cdot 3600 = 31{,}536{,}000\ s/a \quad \text{(S5b)}$$

where E is the amount of electricity produced in the year t, Q is the geofluid flow rate in the year t (kg/s) as of Table S1, ρ_{water} is the density of geothermal fluids (1078 kg/m^3), Cp_{water} is the specific heat capacity of geothermal fluids (4250 J/kg·K), T_z is the temperature at depth z, T_r is the base or reference temperature, η_{th} is the thermal efficiency, t_{load} is the time in s/a and presented in Equation S5b, and CF is the average capacity factor for geothermal plants that is set to 0.9.

The assumptions for geothermal cost estimation are listed in Table S1.

Table S1. Assumptions for geothermal cost estimation from 2015 to 2050 [1,3,4].

	2015	2020	2030	2040	2050
Geofluid flow rate (kg/s)	30	50	70	100	100
Fraction of drilling cost (%)	100	100	90	80	70

The net thermal efficiency (η_{th}) is calculated using the Protocol's recommendation [5], as given in Equation S6.

$$\eta_{th}(T_z, T_r) = 0.00052 \cdot T(T_z, T_r) + 0.032 \quad \text{(S6)}$$

The power capacity (W) is then calculated using Equation S7.

$$W(T_z, T_r, \eta_{th}, t) = \frac{E(T_z, T_r, \eta_{th}, t)}{FLH \cdot CF} \quad \text{(S7)}$$

where FLH is the full load hours of a year (8760 h).

For the reservoir stimulation costs ($C_{cap,stim}$), only injection wells are assumed to stimulate with a flat rate of S, which is assumed to be 2.5 mUSD per injection well [1,6]. The maximum number of production wells per injection well is taken at four.

$$C_{cap,stim} = S \quad \text{(S8)}$$

The geothermal fluid distribution costs are the capital costs related to the surface brine gathering system and are estimated as shown in Equation S9.

$$C_{cap,distr}(T_z, T_r, \eta_{th}, t) = 50 \cdot W(T_z, T_r, \eta_{th}, t) \quad \text{(S9)}$$

The resource exploration cost correlation is calculated using Equation S10.

$$C_{cap,expl}(z, T_z, q_0, k, t) = 1.12 \cdot (C_{extra} + 0.6 \cdot C_{cap,well}(z, T_z, q_0, k, t)) \quad \text{(S10)}$$

where the factor 1.12 amounts for the technical and office support expenses, C_{extra} is the amount for non-drilling activities such as geophysical surveys and field work that is assumed to be 1 mUSD, and it is assumed 1 slim-hole well is drilled at 60% of the geothermal well drilling and completion cost. As pointed out by Beckers et al. [1], this correlation is just an assumption and will not represent the actual exploration cost of every EGS project.

To assess CAPEX trajectories, a learning rate of 7.5% per doubling of the historic cumulative capacity is assumed, which is the average value of the Reference and High scenarios for EGS, according to Tsiropoulos et al. [7]. The learning rate is then used in the learning factor formula employed from Vartiainen et al. [8] and Caldera and Breyer [9], as given in Equation S11.

$$LF(y_0, y_f) = \left(\frac{Cap(y_f)}{Cap(y_0)}\right)^{\frac{\log PR}{\log 2}} \quad \text{(S11a)}$$

$$PR = 1 - LR \quad \text{(S11b)}$$

$$Cap(y_f) = Cap(y_0) \cdot \prod_{t=0}^{t_n} (1 + GR_t) \quad \text{(S11c)}$$

where $Cap(y_f)$ is the historic cumulative capacity projected for the future for the year *t*, $Cap(y_0)$ is the historic cumulative capacity at the reference year, *PR* is the progress ratio, *LR* is the learning rate, and GR_t is the growth rate for the year *t*.

A value of 2% of the estimated CAPEX is considered for the fixed operational expenditure (OPEX), according to the NREL [4] for both flash and binary plants and Carlsson et al. [10] for ORC plants. The variable OPEX is set to zero.

Finally, the levelized cost of electricity (LCOE) is calculated using the Equation S12:

$$LCOE(z, T_r, T_z, \eta_{th}, W, q_0, k, t, y_0, y_f) = \frac{CAPEX(z, T_r, T_z, \eta_{th}, W, q_0, k, t, y_0, y_f) \cdot crf + OPEX_{fixed}(t)}{E(T_z, T_r, \eta_{th}, t)} + OPEX_{var}(t) \quad \text{(S12)}$$

where $OPEX_{fixed}$ is the fixed OPEX in the year *t*, $OPEX_{var}$ is the variable OPEX in the year *t*, *crf* is the capital recovery factor and is obtained using Equation S13.

$$crf = \frac{WACC \cdot (1 + WACC)^N}{(1 + WACC)^N - 1} \quad \text{(S13)}$$

where *WACC* is the weighted average cost of capital which is assumed to be 7%, and *N* is the technical lifetime of power plants, which is assumed to be 30 years.

To calculate the overnight CAPEX (in USD/kW), the estimated CAPEX in Equation S1 is divided by the power capacity (*W*) in Equation S7, as shown in Equation S14.

$$CAPEX_{overnight}(z, T_r, T_z, \eta_{th}, W, q_0, k, t, y_0, y_f) = \frac{CAPEX(z, T_r, T_z, \eta_{th}, W, q_0, k, t, y_0, y_f)}{W(T_z, T_r, \eta_{th}, t)} \cdot 10^3 \quad \text{(S14)}$$

The detailed calculations for five selected sites are presented in the Supplementary Material (spreadsheet file 3).

2. Validation of the model and results

For further discussion of the topic, it is crucial to compare and validate the obtained results with the relevant findings available in the literature. As a first step, the research results are compared with a study conducted for Europe by Chamorro et al. [11]. The result of this comparison is shown in Figures S1 for both the technical and sustainable power capacity estimate. Data points that have an estimated power capacity of zero cannot be illustrated on the log scale in this figure. Also, the European part of Russia is not considered for this comparison. A linear regression relation, $y = \beta x$, has been followed to find the relation between the reference data x and the modeled data y. As can be seen, the coefficient of determination (R-square) is 0.83 for the case of technical potential and 0.91 for sustainable potential. While in both figures a close correlation between the two studies can be observed, the higher R-square for the sustainable potential can be explained by the fact that a similar approach to that of Chamorro et al. [11] has been used in the current study. For the technical potential estimate, the current study used, to some extent, different input data and methods in estimating the power capacity that led to the variations in the results. In particular, the heat flow data was derived from the Atlas of Geothermal Resources in Europe [12] and thermal conductivity was assumed uniformly across Europe at 2.503 W/mK. The latter agrees with the value proposed by the Protocol [5] (2.5 W/mK) for a global mean in situ sediment. It has been discussed that in the absence of specific data for formations, global collations of published data might provide an appropriate estimate [5]. For instance, a study of 7000 samples of plutonic rocks and 13,000 samples of quartz-poor metamorphic rocks showed a mean conductivity of 2.84 and 2.70 W/mK, respectively [13]. After correction for in situ temperature of 175°C, the suggested global mean values are 2.14 and 3.45 W/mK for plutonic and quartz-poor basements, respectively. For the case of this research, the main source of thermal conductivity data is the correlation between geology and thermal conductivity. A high resolution global lithological map (GLiM) [14] is employed and a mean value of thermal conductivity is taken for each lithological formations, as shown in Table 1 of the paper. In this way, almost the same method as proposed by the Protocol has been applied. However, this cannot guarantee that the assumed values are necessarily accurate for all the areas with similar lithological classification.

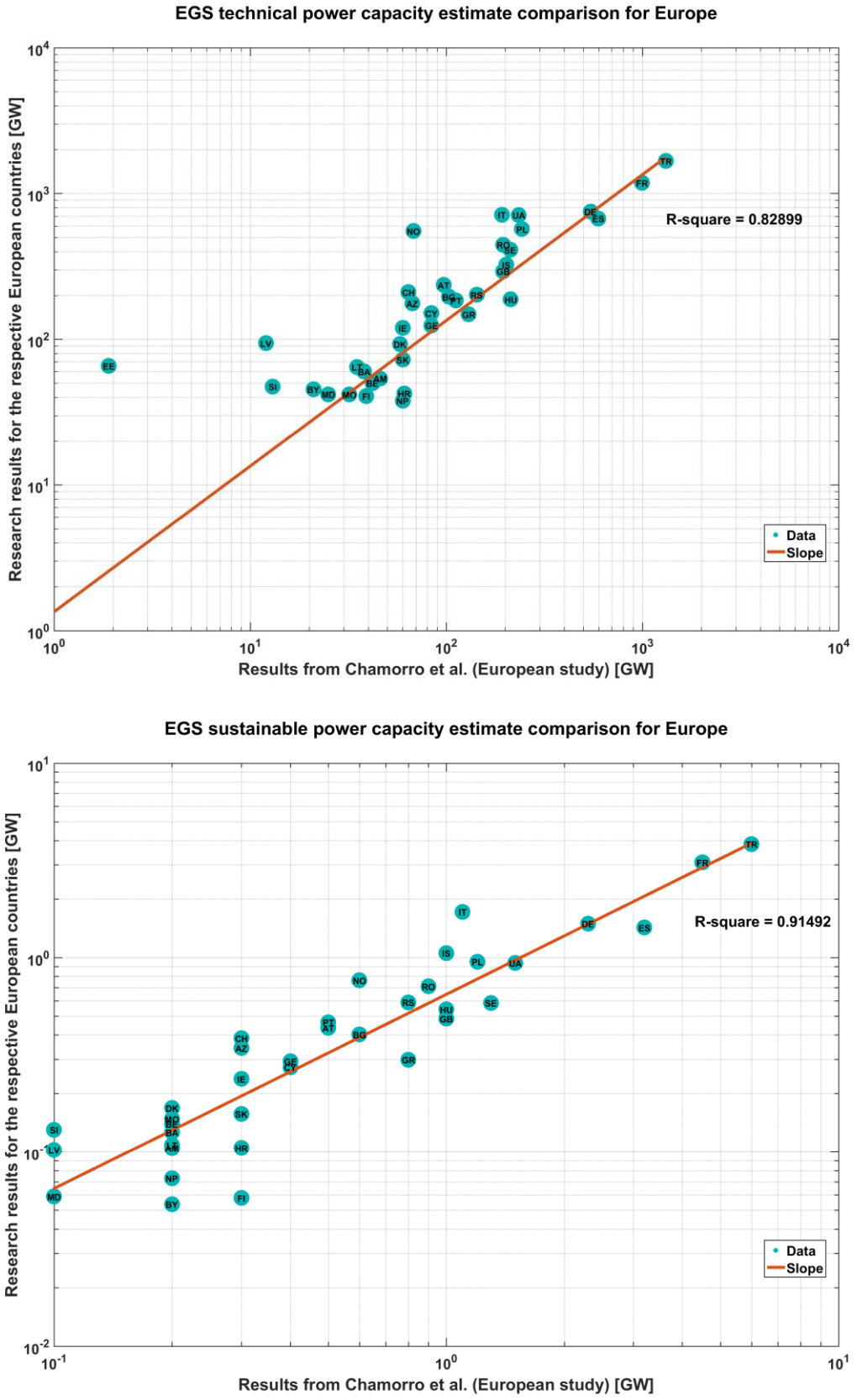

Fig. S1. Comparison of EGS technical (top) and sustainable (bottom) power capacity estimate from this research and Chamorro et al. [11] for European countries.

As discussed by Tester et al. [15], although most of the thermal energy is located in the basement (metamorphic and igneous) rocks under the sedimentary section, the composition and lithology of the basement is extremely variable and even more complex below the sedimentary basin. For instance, the Soultz-sous-Forêts EGS reservoir comprises of two granite types: a porphyritic K-feldspar monzogranite on the depths of 1420 to 4700 m with fractured intermediate section and a two-mica granite on the lowest part [16]. In a general sense, while granite is considered as the most suited rock due to its homogeneity, there might be some layered rocks with equally or more suited fractures than granite for EGS projects. Therefore, understanding the rock characteristics and conditions are crucial for selecting a drilling site. It has been argued that most of the geothermal reservoirs have an analogous porosity per permeability ratio as tight sandstone [17]. This allows to acquire technological knowledge, such as reservoir quality assessment, system optimisation and stimulation, from hydrocarbon resources and apply it for geothermal resources. This reason makes the existing boreholes for gas production more favourable and less expensive for initial EGS development.

Additionally, a comparison is made between the average heat flow data points used for all the countries in Europe. The heat flow data is one of the fundamental components considered for almost all EGS studies. The result is presented in Figure S2. As shown, the coefficient of determination is 0.79, which is in line with the output comparison of this research and Chamorro et al [11]. Table S2 presents the list of abbreviations and full names of all countries used for comparison in Figures S1 and S2.

Table S2. Abbreviations and names of all countries used for the comparison with Chamorro et al. [11].

Country	Abbr.	Country	Abbr.	Country	Abbr.	Country	Abbr.
Albania	AL	Denmark	DK	Italy	IT	Romania	RO
Armenia	AM	Estonia	EE	Latvia	LV	Serbia	RS
Austria	AT	Finland	FI	Lithuania	LT	Slovakia	SK
Azerbaijan	AZ	France	FR	Macedonia	MO	Slovenia	SI
Belarus	BY	Georgia	GE	Moldova	MD	Spain	ES
Belgium	BE	Germany	DE	Montenegro	ME	Sweden	SE
Bosnia and Herzegovina	BA	Greece	GR	Netherlands	NP	Switzerland	CH
Bulgaria	BG	Hungary	HU	Norway	NO	Turkey	TR
Croatia	HR	Iceland	IS	Poland	PL	Ukraine	UA
Czech Republic	CY	Ireland	IE	Portugal	PT	United Kingdom	GB

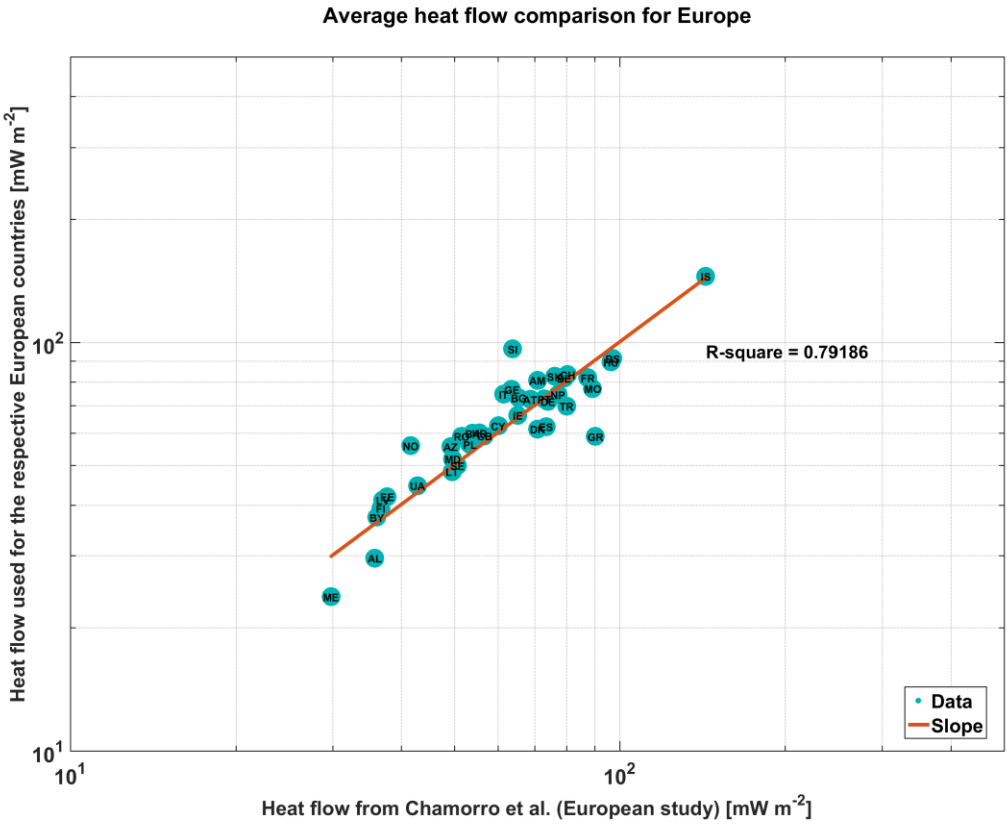

Fig. S2. Comparison of average heat flow data from this research and Chamorro et al. [11] for European countries.

For the second step, the total available heat (thermal energy) content is compared between this research and Tester et al. [15] for the conterminous US states, as shown in Figure S3. The results are found to be more in correlation for the states with greater values, such as Alaska. While the coefficient of determination shows a high value of 88%, the findings in Tester et al. are by a factor of two higher than that found in this research. However, the R-squared value suggests that the model explains approximately 88% of the variability in the response variable of the MIT study. To investigate the reason for such a difference, yet quite close correlation between the two studies, an adjusted R-square has been calculated. As the number of variables in the model increases, a higher R-square can be expected [18]. This can lead to misinterpreting the R-square, as one can increase the number of variables to increase the R-square value. Thus, an alternative approach of looking at adjusted R-square values can be helpful to understand the correlation between the two datasets. The adjusted R-square is quite close to the R-square value with the third digit slightly lower ($R^2 = 0.879$ vs. $R^2_{adj} = 0.876$). This can explain that although the total estimate is lower in the current study than MIT, the correlation between the datasets for different states are comparable. This indicates the relation between the distribution of

resources and input data used to model the temperature at depth as well as the geothermal resource assessment. Table S3 shows the list of abbreviations and full names of all states used for comparison in Figure S3.

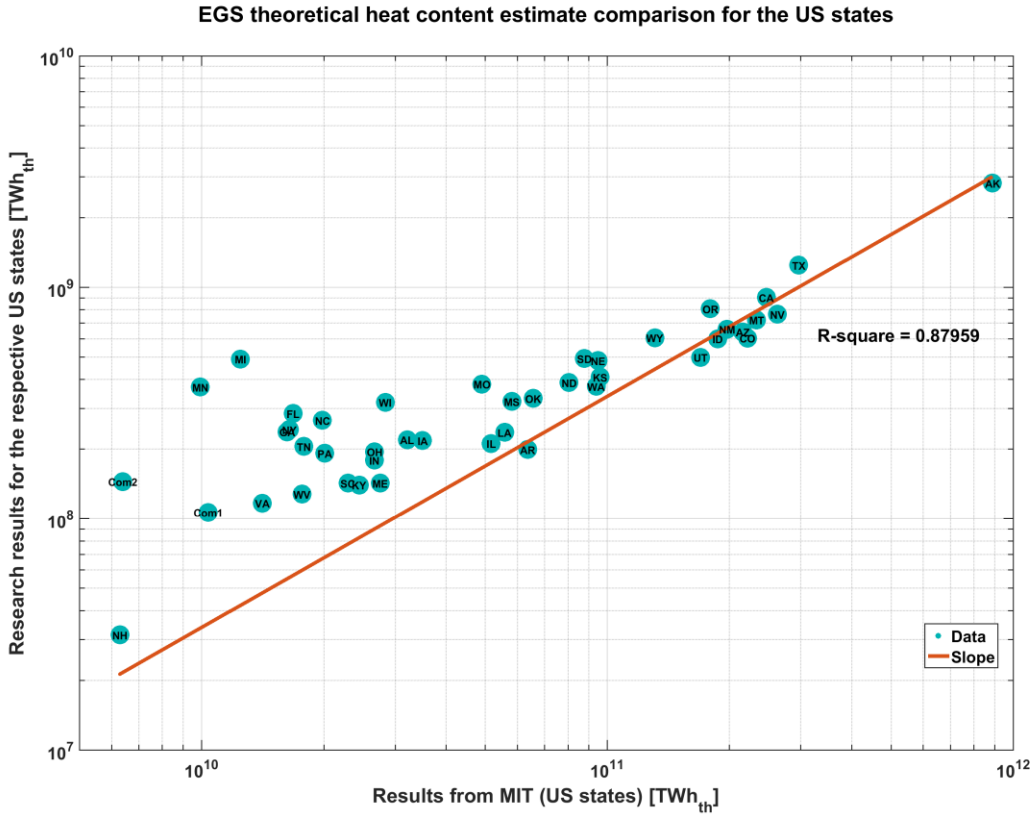

Fig. S3. Comparison of EGS heat (thermal energy) content from this research and Tester et al. [15] for European countries.

Table S3. Abbreviations and names of all states used for the comparison with Tester et al. [15].

State	Abbr.	State	Abbr.	State	Abbr.	State	Abbr.
Alabama	AL	Indiana	IN	Nevada	NV	Tennessee	TN
Alaska	AK	Iowa	IA	New Hampshire	NH	Texas	TX
Arizona	AZ	Kansas	KS	New Mexico	NM	Utah	UT
Arkansas	AR	Kentucky	KY	New York	NY	Virginia	VA
California	CA	Louisiana	LA	North Carolina	NC	Washington	WA
Colorado	CO	Maine	ME	North Dakota	ND	West Virginia	WV
District of Columbia	DC	Michigan	MI	Ohio	OH	Wisconsin	WI
Florida	FL	Minnesota	MN	Oklahoma	OK	Wyoming	WY

Georgia	GA	Mississippi	MS	Oregon	OR	Connecticut, Massachusetts, Rhode Island, Vermont	Com1
Hawaii	HI	Missouri	MO	Pennsylvania	PA	Delaware, Maryland, New Jersey	Com2
Idaho	ID	Montana	MT	South Carolina	SC		
Illinois	IL	Nebraska	NE	South Dakota	SD		

The reason for selecting these two studies is due to the availability of data for a direct comparison, as well as the number of countries/ states that have been analysed.

3. Figures

Additional figures described in the main article are presented below. For detailed information regarding each figure, see the main article. The presented data in this article can be provided upon request.

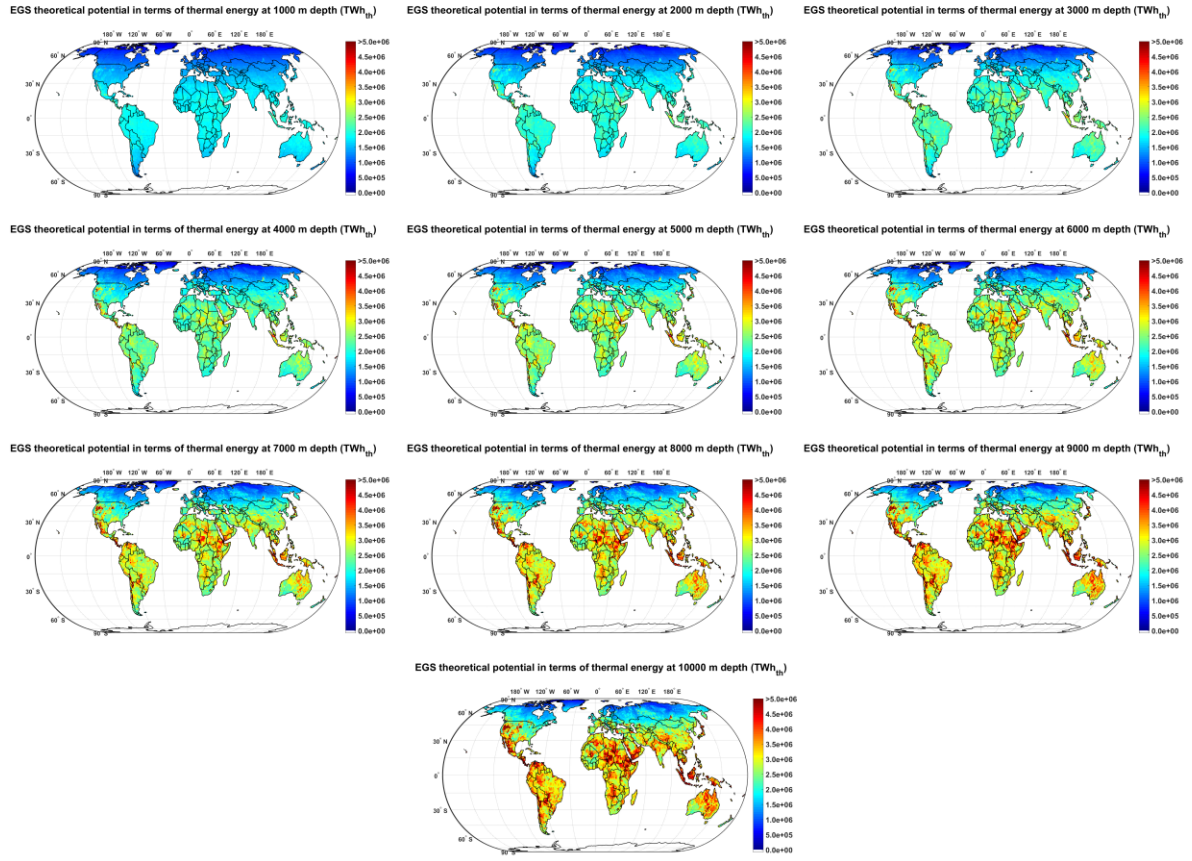

Fig. S4. Global EGS theoretical potential in terms of thermal energy at 1 km depth interval from 1 km up to 10 km of depth.

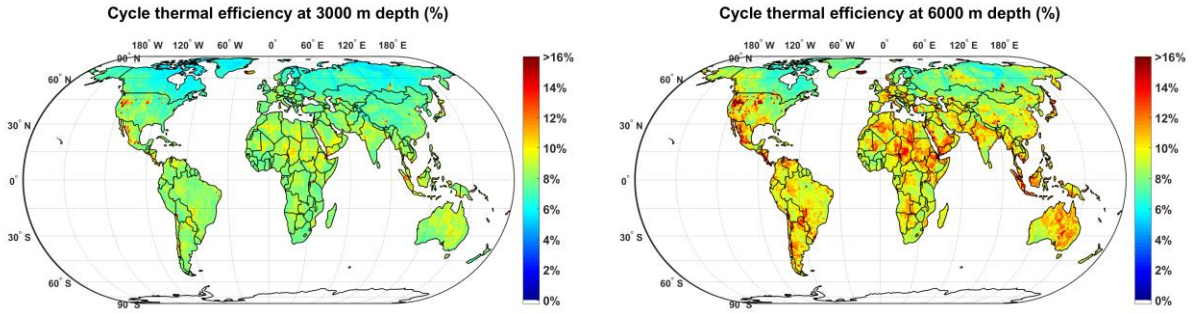

Fig. S5. Exemplary maps representing net thermal efficiency at depths of 3 km (left) and 6 km (right).

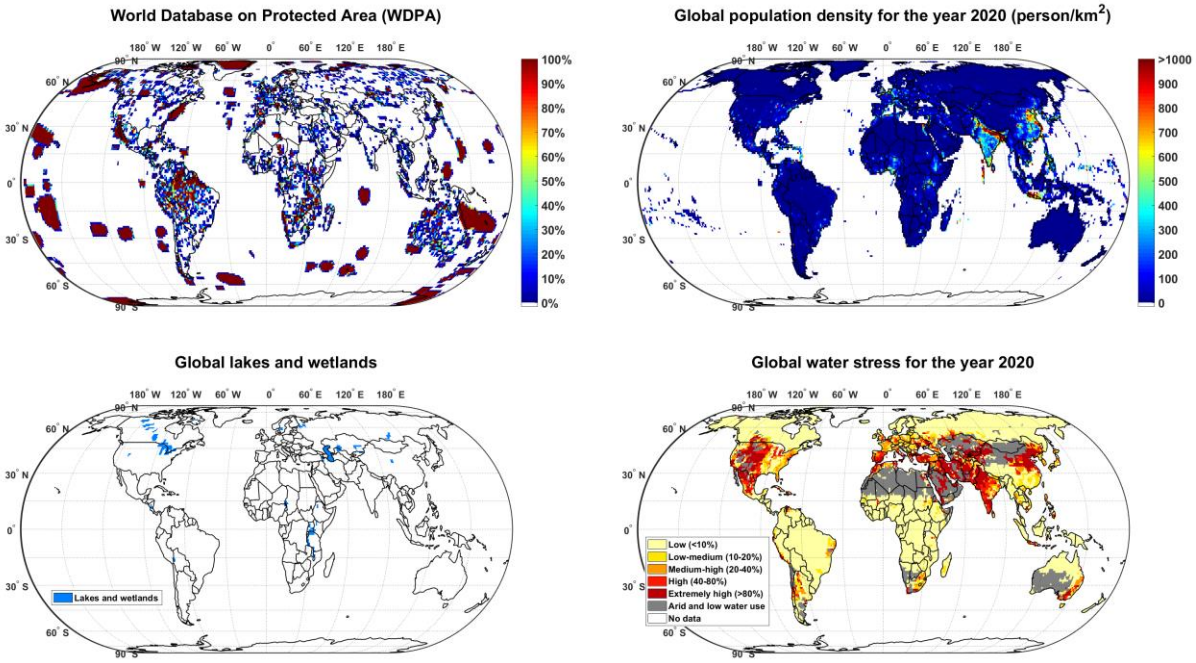

Fig. S6. Main constraints applied to calculate the EGS technical potential, including world database on protected area [19] (top left), global population density for the year 2020 [20] (top right), global lakes and wetlands [21] (bottom left), and global water stress for the year 2020 [22] (bottom right).

References

[1] Beckers KF, Lukawski MZ, Anderson BJ, Moore MC, Tester JW. Levelized costs of electricity and direct-use heat from Enhanced Geothermal Systems. J Renew Sustain Energy 2014;6:013141. https://doi.org/10.1063/1.4865575.

[2] Lukawski MZ, Anderson BJ, Augustine C, Capuano LE, Beckers KF, Livesay B, et al. Cost analysis of oil, gas, and geothermal well drilling. J Pet Sci Eng 2014;118:1–14. https://doi.org/10.1016/J.PETROL.2014.03.012.

[3] Limberger J, Calcagno P, Manzella A, Trumpy E, Boxem T, Pluymaekers MPD, et al. Assessing the prospective resource base for enhanced geothermal systems in Europe. Geotherm Energy Sci 2014;2:55–71. https://doi.org/10.5194/gtes-2-55-2014.

[4] [NREL] - National Renewable Energy Laboratory. 2018 Annual Technology Baseline 2018. https://atb.nrel.gov/electricity/data.html (accessed May 13, 2019).

[5] Beardsmore G, Rybach L, Blackwell D, Baron C. A Protocol for Estimating and Mapping Global EGS Potential. Geotherm Resour Counc Trans 2010;34:301–12.

[6] Mines G, Nathwani J. Estimated Power Generation Costs for EGS. Thirty-Eighth Work. Geotherm. Reserv. Eng., Stanford, California: Stanford University, SGP-TR-198, February 11-13; 2013.

[7] Tsiropoulos I, Tarvydas D, Zucker A. Cost development of low carbon energy technologies - Scenario-based cost trajectories to 2050, 2017 Edition. Luxembourg: EUR 29034 EN, Publications Office of the European Union, JRC109894; 2018. https://doi.org/10.2760/490059.

[8] Vartiainen E, Masson G, Breyer C, Moser D, Román Medina E. Impact of weighted average cost of capital, capital expenditure, and other parameters on future utility-scale PV levelised cost of electricity. Prog Photovoltaics Res Appl 2019:DOI: 10.1002/pip.3189. https://doi.org/10.1002/pip.3189.

[9] Caldera U, Breyer C. Learning Curve for Seawater Reverse Osmosis Desalination Plants: Capital Cost Trend of the Past, Present, and Future. Water Resour Res 2017;53:10523–38. https://doi.org/10.1002/2017WR021402.

[10] Carlsson J, Fortes M del MP, de Marco G, Giuntoli J, Jakubcionis M, Jäger-Waldau A, et al. ETRI 2014 - Energy Technology Reference Indicator projections for 2010-2050. Luxembourg: European Commission; 2014. https://doi.org/10.2790/057687.

[11] Chamorro CR, García-Cuesta JL, Mondéjar ME, Pérez-Madrazo A. Enhanced geothermal systems in Europe: An estimation and comparison of the technical and sustainable potentials. Energy 2014;65:250–63. https://doi.org/10.1016/J.ENERGY.2013.11.078.

[12] Hurter S, Haenel R. Atlas of geothermal resources in Europe. Luxemburg: Publications Office of the European Communities; 2002.

[13] Clauser C. Geothermal Energy. Gr. VIII Adv. Mater. Technol., Heidelberg-Berlin: Vol. 3: Energy Technologies, Subvol. C: Renewable Energies, Springer Verlag; 2006, p. 493–604.

[14] Hartmann J, Moosdorf N. The new global lithological map database GLiM: A representation of rock properties at the Earth surface. Geochemistry, Geophys Geosystems 2012;13:1–37. https://doi.org/10.1029/2012GC004370.

[15] Tester JW, Anderson BJ, Batchelor AS, Blackwell DD, DiPippo R, Drake EM, et al. The Future of Geothermal Energy: Impact of Enhanced Geothermal Systems (EGS) on the United States in the 21st Century. Cambridge, Massachusetts: 2006. https://doi.org/10.1016/j.jbusres.2015.10.046.

[16] Schill E, Meixner J, Meller C, Grimm M, Grimmer JC, Stober I, et al. Criteria and geological setting for the generic geothermal underground research laboratory, GEOLAB. Geotherm Energy 2016;4:7. https://doi.org/10.1186/s40517-016-0049-5.

[17] Moeck IS. Catalog of geothermal play types based on geologic controls. Renew Sustain Energy Rev 2014;37:867–82. https://doi.org/10.1016/j.rser.2014.05.032.

[18] Shieh G. Improved Shrinkage Estimation of Squared Multiple Correlation Coefficient and Squared Cross-Validity Coefficient. Organ Res Methods 2008;11:387–407. https://doi.org/10.1177/1094428106292901.

[19] UNEP-WCMC. Protected areas map of the world 2019. https://www.protectedplanet.net/ (accessed June 13, 2019).

[20] Center for International Earth Science Information Network - CIESIN - Columbia University. Gridded Population of the World, Version 4 (GPWv4): Population Density Adjusted to Match 2015 Revision UN WPP Country Totals, Revision 11 2018. https://doi.org/10.7927/H4F47M65 (accessed May 22, 2019).

[21] Tapiquén CEP. World lakes 2015. http://tapiquen-sig.jimdo.com (accessed May 24, 2019).

[22] Luck M, Landis M, Gassert F. Aqueduct Water Stress Projections: Decadal Projections of Water Supply and Demand Using CMIP5 GCMs, Technical Note. Washington, D.C.: World Resources Institute; 2015. http://www.wri.org/publication/aqueduct-water-stress-projections.